the inverse problem, in the case of uneven sampling only. Aliasing takes place only from small-scale signals to long wavelength signals, whereas leakage may occur both ways. For instance, in the determination of magnetic anomaly maps, it is common to expand the anomaly field into spherical harmonic degrees 15 through 60 (*16*). Without any precautions, there is a possibility of leakage from low-frequency basis functions (below degree 15) as well as from high-frequency basis functions (above degree 60).

Another, more general, way of looking at the effects of leakage is by considering Eq. 6. The first term of the right-hand side defines the classical resolution operator. The additional term on the right-hand side defines the bias introduced by leakage, and its interpretation is similar to that of the resolution operator. It is clear from its expression that the bias operator depends on only the sampling geometry by means of the data kernels and the a priori information (or norm weightings). We calculated the bias operator for the tomography problem discussed above for spherical harmonic degrees 13 through 20. Figure 5 shows the bias operator together with the resolution operator for each degree. Degree 12 (the highest degree of the expansion) is most biased by degree 13 (the first neglected degree), and the spectral leakage is strongest for the spherical harmonic components close to the truncation level. Whereas the weighted least-squares model is almost identical to the true model, the classical least-squares model departs more and more from the true model with each higher degree. With a different approach, Hulot *et al.* (*17*) reached a similar conclusion and found that only the lowest degrees of core motions could be retrieved satisfactorily from geomagnetic data.

The far-reaching conclusions of seismic tomography in terms of geodynamic constraints on the driving forces of mantle convection, petrological models, and mineral physics call for the highest possible precision of the three-dimensional structure of the Earth's interior. The formulation of most seismic tomography problems introduces a bias by leaking basis functions into the solution (Figs. 4 and 5). Accounting for such leakage might change our three-dimensional image of the Earth.

REFERENCES AND NOTES

1. A. Tarantola, *Inverse Problem Theory: Methods for Data Fitting and Model Parameter Estimation* (Elsevier, New York, 1987).
2. R. L. Parker, *Geophysical Inverse Theory* (Princeton Univ. Press, Princeton, NJ, 1994).
3. R. Snieder, J. Beckers, F. Neele, *J. Geophys. Res.* **96**, 501 (1991).
4. R. Snieder, in *Seismic Tomography: Theory and Practice*, H. M. Iyer and K. Hirahara, Eds. (Chapman and Hall, London, 1993), pp. 23–63.
5. C. Spencer, *Geophys. J. R. Astron. Soc.* **80**, 619 (1985).
6. For leakage reduction to be optimal, values for α^2 have to be smaller than those for β^2 without reaching 0. In all our simulations, we used $\alpha^2 = 10^{-6}$ and $\beta^2 = 10^{-3}$.
7. G. E. Backus, *Geophys. J.* **92**, 125 (1988).
8. A. M. Dziewonski and J. H. Woodhouse, *Science* **236**, 37 (1987).
9. J. H. Woodhouse and A. M Dziewonski, *Philos. Trans. R. Soc. London Ser. A* **328**, 291 (1989).
10. B. A. Romanowicz, *Annu. Rev. Earth Planet. Sci.* **19**, 77 (1991).
11. M. H. Ritzwoller and E. M. Lavely, *Rev. Geophys.* **33**, 1 (1995).
12. D. Giardini, X.-D. Li, and J. H. Woodhouse [*J. Geophys. Res.* **93**, 13716 (1988)] worried about the truncation of basis functions in seismic tomography by using normal modes. Snieder *et al.* (*3*) analyzed the origin of the leakage. They referred to the problem as "spectral leakage" because their whole analysis used a spectral basis (spherical harmonics).
13. O. Gudmundsson, J. H. Davis, R. W. Clayton, *Geophys. J. Int.* **102**, 25 (1990).
14. J. Trampert and J. H. Woodhouse, *ibid.* **122**, 675 (1995).
15. R. Bracewell, *The Fourier Transform and Its Applications* (McGraw-Hill, New York, 1965).
16. J. Arkani-Hamed, R. A. Langel, M. Purucker, *J. Geophys. Res.* **99**, 24075 (1994).
17. G. Hulot, J. L. Le Mouël, J. Wahr, *Geophys. J. Int.* **108**, 224 (1992).
18. A. M. Dziewonski and D. L. Anderson, *Phys. Earth Planet. Inter.* **25**, 297 (1981).

19. We would like to thank A. Jackson and J. Woodhouse for many stimulating discussions at earlier stages of this work. J.-J. Lévêque provided many useful comments during the preparation of this manuscript.

17 October 1995; accepted 16 January 1996

Radiation-Induced Diamond Formation in Uranium-Rich Carbonaceous Materials

Tyrone L. Daulton* and Minoru Ozima

Nanometer-sized diamonds were identified by transmission electron microscopy in a uranium-rich, coal-like carbonaceous assemblage of Precambrian age. This observation, together with estimates of formation efficiencies, supports the hypothesis that diamond can form in carbonaceous material irradiated by the radioactive decay products of uranium. The results also suggest that the formation of carbonados cannot be sufficiently explained by a radiation mechanism alone.

Dubinchuk *et al.* (*1*) first reported submicrometer-sized diamonds in uranium-bearing sedimentary rocks with a high carbon content (for example, kerogens, lignite, coal, and kerite) that had never been subjected to high temperatures or pressures; they speculated that diamond was formed when carbonaceous material was irradiated by the spontaneous fission products of uranium. Kaminsky (*2*) extended this idea and proposed that carbonados were also formed by this mechanism. Carbonados are polycrystalline porous aggregates of fine-grained diamonds found only in placer deposits and are characterized by many crustal features, including mineral inclusions of crustal assemblages, tightly trapped atmospheric noble gases, and a lack of association with kimberlites or lamproites. These features strongly suggest that the diamonds did not form by high static pressure in Earth's mantle. One possible mechanism of formation is shock metamorphism resulting from the impact of extraterrestrial bodies (*3*). Carbonados containing the shock-associated diamond polymorph lonsdaleite have been found in meteorite craters (*4*). However, not all carbonados contain lonsdaleite or are associated with established impact structures. A considerable amount of parentless fission Xe and Kr has been identified in Brazilian and African carbonados (*5*). The presence of such large amounts of fissiogenic Xe and Kr is possible only if the carbonaceous precursors to diamond (as well as the diamond itself) were originally part of a finely dispersed U-rich material over geological time scales, consistent with the hypothesis of Kaminsky (*2*). However, the identification of micrometer-sized grains as diamond by Dubinchuk *et al.* (*1*) is tenuous, because the determination was based on electron microdiffraction patterns that yielded unit-cell parameters similar to those of diamond. No stereographic analysis of the diffraction patterns or chemical analysis of the grains was reported.

To evaluate the feasibility of a radiation-induced diamond formation mechanism, Fisenko *et al.* (*6*) studied carburanium, a U-rich (~5% uranium oxides by weight), fine-grained, coal-like assemblage containing hydrous, amorphous carbonaceous material (~65% by weight) of Precambrian age (1.7 ± 0.2 billion years) from North Karelia, Russia (*7*). The carbonaceous grains in carburanium have received high

---

T. L. Daulton, Department of Physics and McDonnell Center for the Space Sciences, Washington University, St. Louis, MO 63130, USA.

M. Ozima, Department of Earth and Planetary Sciences, Washington University, St. Louis, MO 63130, USA, and Department of Earth and Planetary Physics, University of Tokyo, Bunkyo-Ku, Tokyo 113, Japan.

*To whom correspondence should be addressed. Present address: Materials Science Division, Argonne National Laboratory, Argonne, IL 60439, USA.

fluences of energetic particles; therefore, if diamond can be formed by a radiation process, it should be present. Fisenko *et al.* subjected fragments of carburanium to acid-dissolution treatments to isolate any diamond present (8). However, Debye x-ray diffraction failed to detect diamond in these residues (6), indicating that diamond must constitute <10% of the acid-dissolution residue if it were present.

To determine whether diamond was present as a minor phase, we studied the constituent grains in these residues with high-resolution transmission electron microscopy (HRTEM). The carburanium residues contained grains that were about 500 nm in diameter. Roughly 90% of the grains were single crystals, and the remainder were in the form of fine-grained polycrystalline aggregates. Energy-dispersive x-ray spectroscopy indicated that the single crystals were mostly yttrium phosphates and that the fine-grained aggregates (Fig. 1) consisted predominantly of carbon (9). These carbonaceous aggregates produced selected area diffraction patterns (Fig. 2) that exhibited diffraction maxima that indexed well to the maxima of cubic diamond (Fig. 3 and Table 1). In addition to the allowed reflections, the kinematically forbidden (200), (222), and (420) cubic diamond reflections were also present with appreciable intensities; forbidden reflections are often observed in synthesized nanometer-sized diamonds and have been explained in terms of dynamical diffraction effects or lattice distortions arising from atomic impurities (*10–12*). From the intensity of the diamond reflections and the lack of any other strong peaks (*13*), we inferred that these acid residue aggregates consisted predominantly of diamond. The discrete nature of the diffraction rings, which comprised individual reflections that varied in size, indicated that these aggregates contained randomly oriented nanometer-sized diamonds that varied in size by at least an order of magnitude.

HRTEM images of thin (<50 nm) areas near the perimeter of the aggregates revealed diamond grains approaching 40 nm in diameter, some of which exhibited low-angle grain boundaries that indicated intimate contact between the grains. High defect densities were observed in the form of dislocations, platelet-type defects, stacking faults, and twin boundaries; however, defect-free regions were also observed. In addition, euhedral, multiply twinned, nanometer-sized diamonds were observed embedded within amorphous material in the aggregate (Fig. 4). The observation of diamond in the carburanium residue provided additional evidence that carbonaceous material, catastrophically disrupted by energetic particles, can crystallize as diamond. In light of this evidence, we discuss the plausibility of a radiation mechanism for producing diamond and investigate the impli-

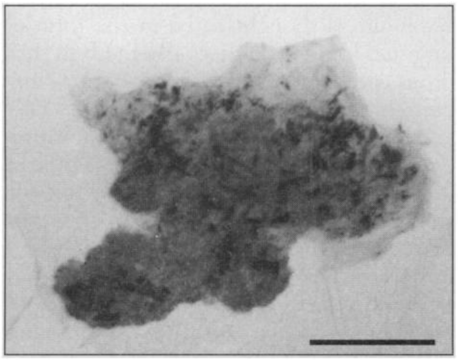

Fig. 1. An inverted-contrast dark-field image of a fine-grained polycrystalline aggregate observed in the carburanium residue. Dark regions correspond to localized areas of strong diffraction resulting from the presence of crystalline material with proper orientation to the incident electron beam to satisfy the Bragg condition. Scale bar, 25.0 nm.

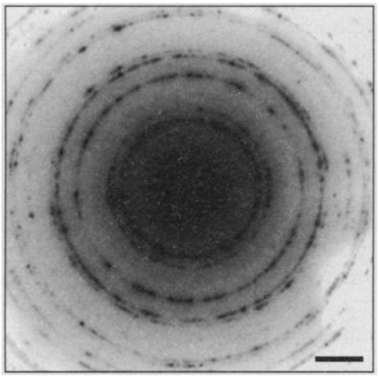

Fig. 2. A selected area diffraction pattern recorded from a fine-grained polycrystalline aggregate present in the carburanium residue. Scale bar, 1/Å.

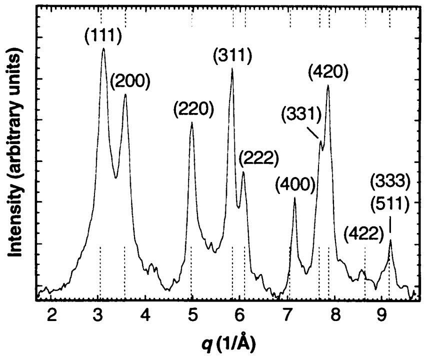

Fig. 3. Selected area diffraction profile. Diffraction intensities were measured along a radial line from the center of the diffraction pattern in Fig. 2 (*q*, reciprocal space reflection). The background intensity was fitted to a power law and subtracted. The presence of diffraction peaks that indexed well to cubic diamond reflections (indicated by dashed lines) is evident. Because of the discrete and broken nature of the diffraction rings, the measured intensities varied with the choice of the radial profile. The plotted intensities are consistent with the average intensities of the broken diffraction rings, with the exception of the (400) reflection, which plots with more intensity than the average intensity of the (400) ring because the profile intersected an intense spot in this ring.

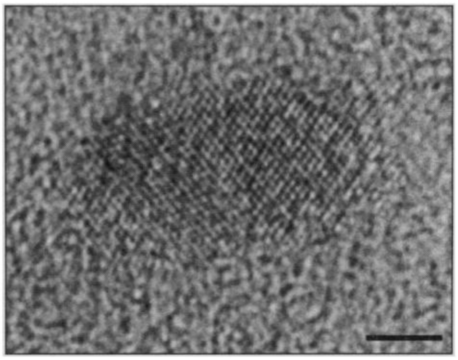

Fig. 4. HRTEM atomic resolution lattice image recorded near the perimeter of an aggregate reveals a multiply twinned nanometer-sized diamond. Twinning along (111) planes is a growth feature commonly observed in nanocrystalline diamond. Scale bar, 2.0 nm.

Table 1. Reciprocal space reflections, *q*, measured from the selected area diffraction pattern of Fig. 2 are compared with those predicted for cubic diamond. Typical error was ±0.03 1/Å. The corresponding *d*-spacings (2π/*q*) for the measured and predicted reflections as well as their difference, δ, are shown for reference.

hkl	Measured		Predicted		|δ| (Å)
	q (1/Å)	2π/*q* (Å)	*q* (1/Å)	2π/*q* (Å)	
(111)	3.074	2.044	3.051	2.059	0.015
(200)*	3.543	1.773	3.523	1.783	0.010
(220)	4.950	1.269	4.983	1.261	0.008
(311)	5.803	1.083	5.843	1.075	0.008
(222)*	6.059	1.037	6.103	1.030	0.007
(400)	7.146	0.879	7.047	0.892	0.013
(331)	7.700	0.816	7.679	0.818	0.002
(420)*	7.850	0.800	7.879	0.798	0.002
(422)	8.575	0.733	8.631	0.728	0.005
(333)/(511)	9.193	0.683	9.154	0.686	0.003

*Forbidden cubic diamond reflections.

cations of such a mechanism for the formation of carbonado.

The initial kinetic energies of ^{238}U fission fragments are about 98 and 67 MeV, which can produce extensive damage in materials (*14*). Tracks of uranium fission fragments observed in muscovite mica are typically 20 μm in length (*15*), and the diameter of their damaged cores is estimated at 2.5 nm (*16*), corresponding to a volume of 10^{-16} cm^3 or $\sim 10^7$ displaced atoms. The rate of ^{238}U α decay is more than six orders of magnitude greater than that of spontaneous fission into two heavy fragments and results in α recoil nuclei ($\sim$100 keV) and α particles ($\sim$4 MeV). However, the range of α recoil nuclei is very short, $\sim$10 nm, less than one-thousandth of that of fission fragments (*17*).

Several theories have been proposed to describe the mechanism by which energetic particles produce catastrophic disruption of solids. Appreciable lattice damage occurs when the total energy dissipation rate of an energetic particle is above some critical value characteristic of the particular solid being traversed (*18*). A high-energy particle traversing a solid will rapidly become stripped of all or some portion of its orbital electrons. At these high energies, the dominant energy-loss mechanism for an ionized particle arises from the Coulomb interactions between the high-velocity ion and the electrons attached to the atoms in the solid; this interaction results in an electrostatically unstable array that breaks apart (*19*). At low energies, the ion recombines with free electrons and the dominant energy-loss mechanism is atomic collisions, resulting in a cascade of lattice displacements (*20*).

The irradiation of coallike material and amorphous hydrogenated carbon results in structural rearrangement; C–H bonds are broken, resulting in the formation of both sp^2 and sp^3 C–C bonds. The radiochemical dehydrogenation of uranium-rich natural coal was studied by Ergun *et al.* (*21*). Döbeli *et al.* (*22*) showed that the conductivity of amorphous carbon films increased by several orders of magnitude upon irradiation with 15-MeV Cl ions, and they suggested that increased conductivity resulted from the formation of graphite microcrystallites along the tracks. This does not preclude the possibility of the formation of nanometer-sized diamond along with the graphite; resistivity measurements are likely insensitive to the formation of small amounts of nanometer-sized diamond. Under appropriate conditions (proper ion mass, ion energies, and fluences), a carbonaceous target might produce an appreciable amount of nanometer-sized diamonds in addition to graphitic carbons. However, typical diamond formation efficiencies might be relatively low compared with those of graphite; carburanium required acid-dissolution treatments to concentrate diamond sufficiently for detection as a minor phase by HRTEM. This fact could contribute to the lack of observation of diamond in well-studied ion-implanted carbons.

Recent studies have shown that it is not difficult to form nanometer-sized diamonds. In fact, several arguments have been made that for nanometer-sized crystals, diamond would be more stable than graphite (*23*). The synthesis of nanometer-sized diamonds has been achieved with different laboratory techniques, including chemical vapor deposition (*24*), explosive detonation (*25*), and laser irradiation (*11*). The conditions produced by the ionizing radiation of a laser might be similar to those present within the ionized channels formed during the intense, short-duration heating events produced as high-energy fission fragments penetrate solid carbonaceous material. Moreover, the rapid thermal quenching that results from contact with the bulk material may favor the formation of metastable phases. Therefore, it is possible that diamond might recrystallize from a catastrophically disordered region produced by an energetic heavy ion.

The mass fraction of nanometer-sized diamonds that could form in carburanium by the interaction of spontaneous decay fragments of uranium with carbonaceous grains can be estimated. The average number of fission fragments that interact with carbonaceous grains depends on the size distribution of the uranium oxide grains and their dispersion in the carbonaceous assemblage. The number of α recoil nuclei that interact with carbonaceous grains is more critically dependent on these details because of their limited range (10 nm); only a fraction may escape the uranium oxide grains. Consequently, α recoil nuclei could reach less carbonaceous material in the carburanium assemblage and would likely affect only the outermost surfaces of the carbonaceous grains.

Within the tracks of disrupted carbon atoms, the total number of nanometer-sized diamonds (N_D) produced by fission fragments and α recoil nuclei is given by

$$N_D = \left(2\nu_f\chi_f\frac{\lambda_f}{\lambda} + 8\nu_\alpha\chi_\alpha\right)N_U(e^{\lambda t} - 1) \quad (1)$$

where $\lambda_f = 8.46 \times 10^{-17}$ year^{-1} and $\lambda = 1.55 \times 10^{-10}$ year^{-1} (*26*); these are the ^{238}U decay constants for spontaneous fission and total decay (α + fission), respectively. N_U is the number of undecayed ^{238}U atoms in the carburanium specimen, t is the age of the carburanium, ν_f is the fraction of fission fragments that interact with carbonaceous grains, and χ_f is the average efficiency of diamond formation per fission fragment. The formation of more than one nanometer-sized diamond per fission fragment (on average) corresponds to $\nu_f\chi_f > 1$, whereas $\nu_f\chi_f < 1$ corresponds to the formation of one nanometer-sized diamond for several fission fragments (on average). The parameters ν_α and χ_α are defined similarly for α recoil nuclei. The total mass of diamond formed (M_D) can be expressed as

$$M_D = \frac{4}{3}\pi r^3 \rho N_D \quad (2)$$

where ρ is the density of diamond and r is an effective spherical radius corresponding to the average volume of the nanometer-sized diamonds. HRTEM results indicated 1 nm $\leq r \leq$ 20 nm; a conservative estimate of r = 8 nm ($\sim 3.8 \times 10^5$ atoms) yielded an M_D of $0.92\ \nu_f\chi_f + 6.7 \times 10^6\ \nu_\alpha\chi_\alpha$ mg, or $\sim 0.92\ \nu_f\chi_f + 6.7 \times 10^6\ \nu_\alpha\chi_\alpha$ for the mass fraction of the carburanium acid residue that can be in the form of diamond.

The relative contributions to diamond formation from fission fragments and α recoil nuclei are heavily dependent on geometrical factors. The uranium in carburanium is thought to be in the form of uranium oxides, either absorbed in hydrous carbon compounds or present as discrete micrometer-sized grains (*27*). Discrete grains represent the most limiting case for interaction with carbon. If 50 μm is used as a conservative upper limit for the uranium oxide grain size, the fractions of decay fragments that escape the uranium grains are, respectively, $\nu_f > 0.8$ and $\nu_\alpha > 6 \times 10^{-4}$. The mass fraction of diamond estimated in the carburanium residue (<0.03% by weight) suggests $\chi_f < 0.14x$ and $\chi_\alpha < 2.5 \times 10^{-5}(1 - x)$, where x reflects the relative contribution to diamond formation by fission fragments and α recoil nuclei. Because modest formation efficiencies can account for the mass of diamonds observed, it appears plausible that a radiation mechanism can produce nanometer-sized diamonds.

The nature of the diamond observed in carburanium is different from that in carbonado. Carbonado aggregates as large as 800 carats (160 g) with less than 20% of their volume in the form of mineral inclusions have been found (*28*); the individual diamond crystallites in carbonado aggregates can reach 20 μm (*29*). In contrast, carburanium contains a dispersion of $\sim$500-nm polycrystalline aggregates comprising nanometer-sized diamond crystals, and the fraction of diamond present in bulk carburanium is <0.003% by weight.

Carburanium represents an ideal natural environment for radiation-induced diamond formation because it is a fine-grained, U-rich carbonaceous material with an exposure age that is about onethird the age of Earth. Nevertheless, the mass fraction of diamond observed in carburanium is several orders of magnitude smaller than that of carbonado. This presents a serious difficulty if a radiation process is to account for carbonado formation. Mass transport problems must be addressed; because <20% of the volume of carbonado is not diamond, some transport mechanism would have to concentrate diamond grains into large aggregates while removing the displaced uranium oxides and decay products. Because carburanium contains 500-nm polycrystalline aggregates, a sintering mechanism would then be required to coalesce these radiation-formed aggregates into the micrometer-sized single crystal grains typical of carbonado. These factors indicate that a radiation mechanism alone cannot satisfactorily explain the formation of carbonado.

REFERENCES AND NOTES

1. V. T. Dubinchuk, A. V. Kochenov, V. F. Penkov, G. A. Sidorenko, V. A. Uspenskiy, *Dokl. Akad. Nauk SSSR Earth Sci. Sect.* **231**, 114 (1976).
2. F. V. Kaminsky, *Dokl. Akad. Nauk SSSR* **294**, 439 (1987).
3. V. J. Smith and J. B. Dawson, *Geology* **13**, 342 (1985).
4. C. Frondel and U. B. Marvin, *Nature* **214**, 587 (1967).
5. M. Ozima, S. Zashu, K. Tomura, Y. Matsuhisa, *ibid.* **351**, 472 (1991).
6. A. V. Fisenko *et al.*, *Proc. Lunar Planet. Sci. Conf.* **24**, 483 (1993); A. V. Fisenko, L. F. Semenova, A. B. Verkhovskii, Y. A. Shukolyukov, *Astron. Lett.* **20**, 56 (1994).
7. Carburanium occurs as brittle, hygroscopic oval inclusions (1 to 3 cm, ρ = 1.6 g/cm^3) within pegmatitic veins 8 to 15 m thick (composed primarily of coarse-grained olivine and quartz) situated among gray gneisses. Carburanium sometimes replaces uranitite crystals or forms a crust on their surface.
8. Fragments with a starting mass of 3.3 g were treated with HNO_3 plus HCl at 20° and 40°C, $K_2Cr_2O_7$ at 80°C, $HClO_4$ at 140° and 220°C, and HCl at 60°C, producing ~1 mg of white residue.
9. The polycrystalline aggregates were >95 atomic % C with trace amounts of Si, O, Fe, Al, Mg, and Ti. The yttrium phosphate crystals exhibited trace amounts of Dy, Er, Gd, and Yb. Carburanium is usually associated with rare-earth minerals such as zirtolite, xenotime, monazite, and uraninite.
10. M. Frenklach *et al.*, *J. Appl. Phys.* **66**, 395 (1989).
11. P. R. Buerki and S. Leutwyler, *ibid.* **69**, 3739 (1991).
12. K. S. Harshavardhan, R. S. Yalamanchi, L. K. Rao, *Appl. Phys. Lett.* **55**, 351 (1989).
13. No graphite was observed in the residues, indicating its complete dissolution by the acid treatments.
14. I. Halpern, *Annu. Rev. Nucl. Sci.* **9**, 245 (1959).
15. G. Bigazzi, *Earth Planet. Sci. Lett.* **3**, 434 (1967).
16. P. B. Price and R. M. Walker, *J. Appl. Phys.* **33**, 3407 (1962).
17. W. H. Huang and R. M. Walker, *Science* **155**, 1103 (1967).
18. R. L. Fleischer, P. B. Price, R. M. Walker, *Phys. Rev.* **133**, A1443 (1964).
19. ______, *J. Appl. Phys.* **36**, 3645 (1965).
20. J. A. Brinkman, *Am. J. Phys.* **24**, 246 (1955).
21. S. Ergun, W. F. Donaldson, I. A. Breger, *Fuel* **39**, 71 (1960).
22. M. Döbeli, T. J. Jones, A. Lee, R. P. Livi, T. A. Tombrello, *Radiat. Eff. Def. Solids* **118**, 325 (1991).
23. J. A. Nuth III, *Astrophys. Space Sci.* **139**, 103 (1987); P. Badziag, W. S. Verwoerd, W. P. Ellis, N. R. Greiner, *Nature* **343**, 244 (1990).
24. M. Frenklach *et al.*, *Appl. Phys. Lett.* **59**, 546 (1991).
25. N. R. Greiner, D. S. Phillips, J. D. Johnson, F. Volk, *Nature* **333**, 440 (1988).
26. R. H. Steiger and E. Jager, *Earth Planet. Sci. Lett.* **36**, 359 (1977).
27. M. V. Soboleva and I. N. Pudovkina, *Mineraly urana* [*Uranium Minerals*] (Gosgeoltekhizdat, Moscow, 1957).
28. L. F. Trueb and W. C. Butterman, *Am. Mineral.* **54**, 412 (1969).
29. L. F. Trueb and E. C. de Wys, *Science* **165**, 799 (1969).

30. We thank Y. Shukolyukov and A. Fisenko for providing the carburanium acid residues and T. Bernatowicz and R. Walker for valuable comments.

26 September 1995; accepted 28 December 1995

Impact Origin of the Chesapeake Bay Structure and the Source of the North American Tektites

Christian Koeberl,* C. Wylie Poag, Wolf Uwe Reimold,
Dion Brandt

Seismic profiles, drill core samples, and gravity data suggest that a complex impact crater ~35.5 million years old and 90 kilometers in diameter is buried beneath the lower Chesapeake Bay. The breccia that fills the structure contains evidence of shock metamorphism, including impact melt breccias and multiple sets of planar deformation features (shock lamellae) in quartz and feldspar. The age of the crater and the composition of some breccia clasts are consistent with the Chesapeake Bay impact structure being the source of the North American tektites.

The recently discovered Chesapeake Bay structure is a complex peak-ring crater buried 300 to 500 m beneath the lower Chesapeake Bay, its surrounding peninsulas, and the adjacent inner continental shelf (*1*). The crater is centered at 37°16.5′N and 76°0.7′W, near the town of Cape Charles on Virginia's segment of the Delmarva Peninsula (Fig. 1). The existence of this unusual circular structure was determined on the basis of 10 multichannel seismic-reflection profiles transecting the bay and 3 single-channel profiles on the inner continental shelf, as well as 56 bore holes drilled inside and outside the crater rim (*1*). The seismic profiles define the outer rim of the structure, which is 90 km in diameter and is marked by concentric normal faults that dip down toward the crater (Fig. 2). A flat-floored annular trough 300 to 1200 m deep separates the outer rim from an irregular, low-relief peak ring (maximum height, ~175 m) (*1*). The peak ring, in turn, encircles a 30-km-wide inner basin with an estimated depth of ≤1.2 km.

Correlation of bore-hole stratigraphy with seismic reflection profiles showed that the preimpact coastal plain rocks consisted of a seaward-thickening wedge of mainly Lower Cretaceous to upper Eocene, poorly lithified, and mainly siliciclastic sedimentary rocks (Fig. 2). The sedimentary sequence rests on a crystalline basement complex comprising granitic and metasedimentary rocks of Proterozoic to Paleozoic age (*2*). Flexural downwarping due to thermotectonism and sediment loading (*3*) has tilted the surface of the crystalline basement eastward toward the axis of the Baltimore Canyon trough (*4*). The seismic profiles indicate that the floor of the eastern sector of the annular trough also steepens eastward, and as a result the trough is deeper in the east (Fig. 2). The faulted rim of the structure has undergone similar differential eastward subsidence.

Bore-hole samples showed that the structure is partly filled with a unit termed the Exmore breccia, which is mainly composed of autochthonous sedimentary clasts in a sandy matrix but also contains millimeter- to centimeter-sized basement clasts

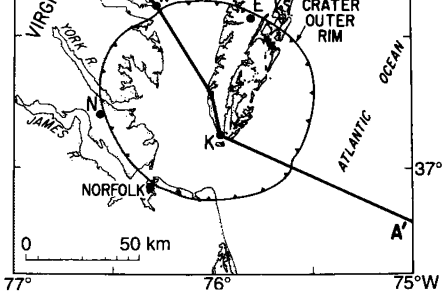

Fig. 1. Location map showing the crater rim as defined by seismic reflection profiles and drill cores. A-A′ is cross section shown in Fig. 2. Solid dots are drill core locations: N, Newport News; W, Windmill Point; E, Exmore; K, Kiptopeke.

C. Koeberl, Institute of Geochemistry, University of Vienna, Althanstrasse 14, A-1090 Vienna, Austria.
C. W. Poag, U.S. Geological Survey, Woods Hole, MA 02543, USA.
W. U. Reimold and D. Brandt, Department of Geology, University of the Witwatersrand, Johannesburg 2050, South Africa.

*To whom correspondence should be addressed.